ACS APPLIED MATERIALS & INTERFACES

Research Article

www.acsami.org

Rapid and Selective Detection of Pathogenic Bacteria in Bloodstream Infections with Aptamer-Based Recognition

Haijing Shen,[†] Jie Wang,[†] Haoyang Liu,[†] Zhihao Li,[†] Fenglei Jiang,[†] Fu-Bing Wang,[‡] and Quan Yuan*[,†]

[†]Key Laboratory of Analytical Chemistry for Biology and Medicine (Ministry of Education), College of Chemistry and Molecular Sciences, Wuhan University, Wuhan, P. R. China

[‡]Department of Laboratory Medicine & Center for Gene Diagnosis, Zhongnan Hospital, Wuhan University, Wuhan, P. R. China

Supporting Information

ABSTRACT: Sepsis and bacteremia are life-threatening clinical syndromes associated with significant patient morbidity and mortality. Rapid and sensitive detection of pathogenic bacteria is the key to improve patient survival rates. Herein, we have rationally constructed a simple aptamer-based capture platform to shorten the time needed for confirmation of bacterial bloodstream infection in clinical blood samples. This capture platform is made of a mesoporous TiO_2-coated magnetic nanoparticle and is modified with target aptamer. It features excellent bacterial enrichment efficiency of about 80% even at low bacterial concentrations (10−2000 CFU mL^{-1}). More importantly, the bacteria can be enriched within 2 h, and the time for bacterial identification is effectively shortened in comparison to the "gold standard" in clinical diagnosis of bloodstream infection. The aptamer-based capture platform may pave a way for the detection of biomarkers and find potential applications in disease diagnosis.

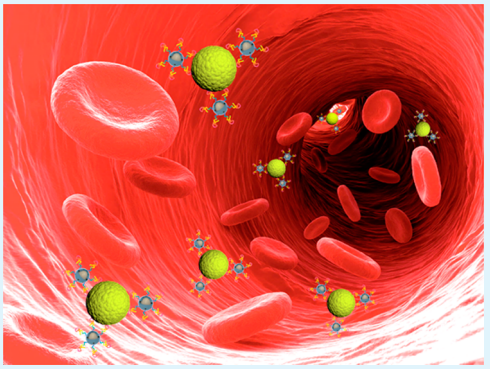

KEYWORDS: *bloodstream infection, bacteria, sepsis, aptamer, magnetic nanoparticle*

INTRODUCTION

Sepsis and bacteremia caused by bacterial bloodstream infections (BSI) are defined as complex clinical syndromes that lead to vascular leakage, tissue damage, and multiorgan failure. The aforementioned syndromes as well as other infectious diseases are potentially life-threatening conditions and are associated with one-third of global mortality.[1−3] The most prevalent causes of BSI are coagulase-negative staphylococci, *Staphylococcus aureus*, *Escherichia coli*, *Pseudomonas aeruginose*, and so on.[4,5] Due to the very low infectious dose (about 100 cells mL^{-1}), it is still a challenge to detect pathogenic bacteria directly from unprocessed blood samples, which contain billions of blood cells and protein, including red blood cells (RBCs or erythrocytes), white blood cells (WBCs or leukocytes), hemoglobin (HGB), and platelets (PLT).[6,7] Currently, broth-based blood culture is the "gold standard" in clinical diagnosis of BSI and is also a prerequisite for additional downstream microbiology testing.[8−10] Typically, the culture bottles containing patient blood are incubated for 3−5 days within a continuous blood culture system. The growth of bacteria is monitored by measuring metabolite production. Upon blood culture positivity, bacterial samples have to grow at least 12 h on solid media to reach a definitive bacterial identification. Subsequently, antibiotic susceptibility tests are performed to guide the appropriate antibiotic therapy. This approach is time-consuming and usually requires several days to report the final outcomes. However, the inability to diagnose pathogenic bacteria rapidly in the early stage of infection is one of the main causes of high mortality.[11−13] As the consensus has been reached that every hour of delay in administration of effective antibiotic therapy results in a 7.6% mean decrease in survival rate,[14,15] it is an urgent demand to develop new diagnostic methods for selective and rapid pathogen detection directly from blood samples. Nowadays, amplification-based molecular diagnostic methods such as fluorescent in situ hybridization[16−18] and real-time polymerase chain reactions[19−21] have been used to effectively shorten the time for bacterial identification following blood culture positivity. Nonetheless, these methods also involve long-term blood culture. More recently developed methods, including surface-enhanced Raman scattering,[22−24] fluorescent probes,[25−28] and nuclear magnetic resonance,[29] have achieved high sensitivity and selectivity in detection of pathogenic bacteria. For example, He et al. used the developed 4-mercaptophenylboronic acid-modified SERS chip to simultaneously capture, analyze, and sterilize bacteria from human blood, reporting a capture efficiency of about 60% at low bacterial concentrations.[24] Zhao et al. integrated DNAzyme-based sensors and IC three-dimensional (3D) technology that could detect bacteria directly from blood with single-cell sensitivity.[28] However, the existing methods require tedious work (cytolysis, nucleic acid extraction, etc.) and expensive equipment, which limits their

Received: June 4, 2016
Accepted: July 14, 2016
Published: July 14, 2016

DOI: 10.1021/acsami.6b06671
ACS Appl. Mater. Interfaces 2016, 8, 19371−19378

Scheme 1. Schematic Representation of Strategies to Identify Pathogens in Human Blood[a]

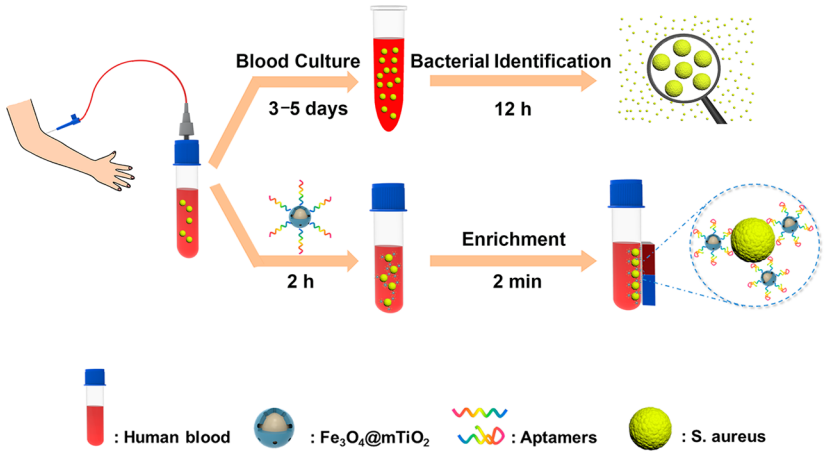

[a]Top: blood culture. Bottom: the aptamer-based capture platform.

widespread use in practical applications. Aptamers are single-stranded DNA or RNA oligonucleotides that are capable of binding to variety of targets with high selectivity and strong affinity by folding into a sequence-defined unique structure.[30−32] Compared to other functional biomolecules, aptamers offer excellent merits, including small size, lack of immunogenicity, easy modification, and ability to be synthesized in bulk amounts. Aptamers have had important applications in target detection, drug delivery, and medical diagnosis.[33−35] Recently, several bacterial aptamers with high selectivity and strong affinity have been isolated through systematic evolution of ligands via exponential enrichment (SELEX).[36,37] Inspired by its high selectivity and strong binding affinity, the aptamer is an ideal option to isolate bacteria from blood samples for rapid detection of pathogenic bacteria.

Herein, we have rationally constructed a simple capture platform made of a mesoporous TiO_2-coated magnetic nanoparticle functionalized with the target aptamer (designated as Apt-Fe_3O_4@mTiO_2), aiming to shorten the time needed for confirmation of BSI as well as pathogen identification. This capture platform integrates the capabilities of bacterial recognition, capture, and enrichment.[38−40] In this approach, Apt-Fe_3O_4@mTiO_2 nanoparticles are incubated with fresh blood from the patient for bacterial enrichment. Once exposed to target bacteria, the aptamer will bind to target bacteria with high selectivity and strong affinity. The bacteria captured by Apt-Fe_3O_4@mTiO_2 nanoparticles are further concentrated by a magnetic field to confirm the bacterial infection and identify pathogenic bacteria (Scheme 1). As a proof of concept test, Gram-positive bacteria *S. aureus* and Gram-negative bacteria *E. coli* were chosen as model bacteria.[41,42] The designed platform features a favorable bacterial-capture efficiency of about 80% even at low infectious doses (10−2000 CFU mL^{-1}). Further, the designed capture platform has little cross-reaction with the nontarget components in blood, revealing its ability for specific enrichment and detection of bacteria in blood. More importantly, the bacteria can be enriched within 2 h, which effectively shortens the time needed for bacterial identification in comparison to that for traditional blood culture. It is worth noting that this capture platform is able to concentrate different bacteria as well as other biomarkers by changing only the aptamer types. These advantages make this aptamer-based capture platform an appealing choice for future development of disease diagnosis.

EXPERIMENTAL SECTION

Aptamers. The sequences of the two aptamers used in this work are listed as follows:

Apt-*S. aureus*: 5′-TCC CTA CGG CGC TAA CCC CCC CAG TCC GTC CTC CCA GCC TCA CAC CGC CAC CGT GCT ACA AC TTT TTT TTT-$(CH_2)_7$-NH_2-3′,

5′-TCC CTA CGG CGC TAA CCC CCC CAG TCC GTC CTC CCA GCC TCA CAC CGC CAC CGT GCT ACA AC TTT TTT TTT-$(CH_2)_7$-FAM-3′, and

Apt-*E. coli*: 5′-ATCC GTCA CACC TGCT CTAC TGGC CGGC TCAG CATG ACTA AGAA GGAA GTTA TGTG GTGT TGGC TCCC GTAT TTT TTT TTT-$(CH_2)_7$-NH_2-3′.

Synthesis and Characterization of Fe_3O_4 Nanoparticles. The hydrophilic Fe_3O_4 nanoparticles were synthesized following the previously reported method.[43,44] Briefly, 1.625 g of $FeCl_3 \cdot 6H_2O$, 0.65 g of trisodium citrate, and 3.0 g of sodium acetate were dissolved in 50 mL ethylene glycol under continuous stirring. After that, the as-prepared yellow solution was sealed into a Teflon-lined stainless-steel autoclave and was heated to 200 °C for 10 h. Then, the obtained nanoparticles were thoroughly washed with ethanol and deionized water three times. The morphology of the synthesized Fe_3O_4 nanoparticles (NPs) was characterized by transmission electron microscopy (TEM).

Synthesis and Characterization of Mesoporous Fe_3O_4@mTiO_2 Core−Shell Nanoparticles. The core−shell structures were obtained following the method described by Zhao and co-workers in their previous research.[45−47] The mesoporous TiO_2 shell was uniformly grown on the surface of Fe_3O_4 NPs in a kinetics-controlled manner. In detail, 150 mg of the aforementioned Fe_3O_4 nanoparticles and 0.3 mL of a 28% w/w concentrated ammonia solution were dispersed in 100 mL of absolute ethanol under constant sonication for 30 min. After that, 0.75 mL of tetrabutyl titanate was added dropwise into the solution within 5 min, and the mixture was reacted at 45 °C for 24 h under continuous mechanical stirring. The as-prepared nanoparticles were washed with water and ethanol three times using a magnet. Subsequently, the prepared products were dried at 100 °C overnight and then calcined at 500 °C for 2 h to improve the crystallinity of the TiO_2 shell as well as to remove the organic species. The morphologies and the phase of the Fe_3O_4@TiO_2 and Fe_3O_4@mTiO_2 nanoparticles were characterized by TEM and X-ray diffraction (XRD), respectively.

Preparation of the Aptamer-Conjugated Fe_3O_4@mTiO_2 Nanocomposites. To selectively enrich bacteria from human blood, the surfaces of mesoporous Fe_3O_4@mTiO_2 nanoparticles were modified with the bacteria-specific aptamer. Fe_3O_4@mTiO_2 (50

DOI: 10.1021/acsami.6b06671
ACS Appl. Mater. Interfaces 2016, 8, 19371−19378

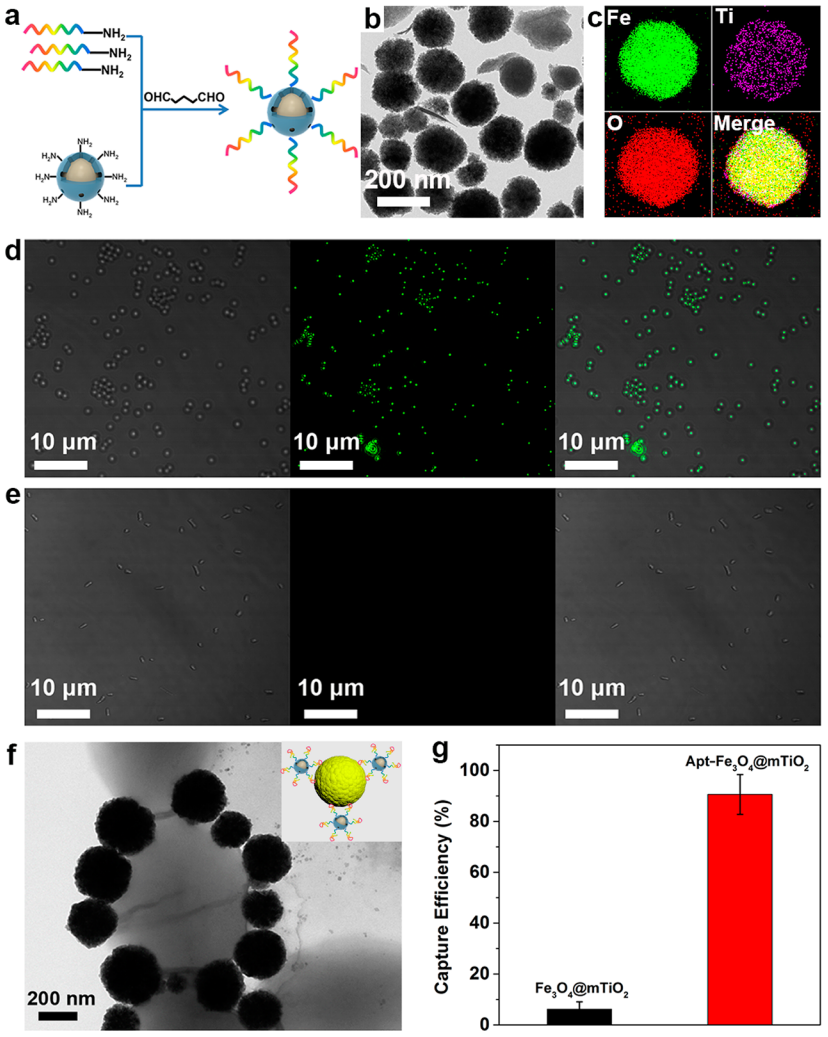

Figure 1. (a) Schematic illustration of the strategy used to prepare the aptamer-based capture platform. (b) TEM image. (c) Elemental mapping images of the Apt-Fe_3O_4@$mTiO_2$ nanoparticles. Confocal fluorescence micrographs of (d) *S. aureus* and (e) *E. coli* after incubation with FAM-$Apt_{S.\ aureus}$. The left, middle, and right images show the bright field, fluorescence, and merged images, respectively. (f) TEM image of *S. aureus* conjugated by $Apt_{S.\ aureus}$-Fe_3O_4@$mTiO_2$. Inset of (f) is the binding model of *S. aureus* and the nanoparticles. (g) Capture efficiency of pure Fe_3O_4@$mTiO_2$ and Apt-Fe_3O_4@$mTiO_2$.

mg) in a 25 mL acetone solution was heated to reflux with stirring, and then 150 μL of 3-aminopropyltriethoxysilane (APTES) was added to introduce amino groups on the surface of Fe_3O_4@$mTiO_2$. After 10 h of stirring, the obtained nanoparticles were thoroughly washed with acetone and dried at 120 °C. After that, the highly established glutaraldehyde spacer method was employed to covalently modify the aptamer onto the surface of the amine-coated Fe_3O_4@$mTiO_2$.[48−50] In brief, 5 mg of amine-coated Fe_3O_4@$mTiO_2$ was incubated with 10 nmol of amine group-labeled aptamer in 5 mL of Tris-HCl buffer at 37 °C overnight. To remove the excess aptamer, the as-prepared $Apt_{S.\ aureus}$-Fe_3O_4@$mTiO_2$ complexes were washed with Tris-HCl buffer three times. The $Apt_{E.coli}$-Fe_3O_4@$mTiO_2$ nanoparticles were also obtained with the same procedure. The successful modification of the aptamers was confirmed by dynamic light scattering (DLS).

Bacterial Sample Culture. The strains of *S. aureus* and *E. coli* were cultured with Luria−Bertani (LB) broth at 37 °C overnight, and the bacterial concentration was determined by the plate dilution method.[51] In brief, the bacterial suspensions were serially diluted and subsequently plated on agar plates in 3−5 replicates. In addition, the colony forming units (CFUs) were also determined by measuring the optical density (OD) at 600 nm (OD_{600} = 1.0 is approximately 1.0 × 10^9 CFU mL^{-1}).[52] In detail, we first diluted the culture to obtain an appropriate OD value of about 1.0. After that, the bacterial solution with an OD_{600} value of about 1.0 was serially diluted and inoculated onto the solid medium to quantify the CFU mL^{-1}.

Confocal Imaging of *S. aureus* and *E. coli* Binding with FAM-Labeled Aptamer. The fluorescein amidite (FAM)-labeled aptamer[39,53] target to *S. aureus* (FAM-Apt, 300 nM) was incubated with 200 μL of bacterial suspension (OD_{600} = 1.0) under protection from light for 45 min with gentle rotation. Then, the bacteria were washed three times with PBS buffer by centrifugation to remove unbound free aptamers. Ten microliters of the redispersed bacteria was dropped on glass slide and covered with a glass coverslip to yield a thin bacterial smear. Obtained bacterial samples were imaged with a confocal laser-scanning microscope.

Transmission Electron Microscopy and Scanning Electron Microscopy Characterization. The bacteria-$Apt_{S.\ aureus}$-Fe_3O_4@$mTiO_2$ complexes were prepared before TEM and SEM observations. First, the bacterial suspension was washed with PBS buffer (pH = 7.4) several times to remove the coated medium. After that, bacterial suspension with an OD_{600} value of 1.0 was incubated with 50 μL of $Apt_{S.\ aureus}$-Fe_3O_4@$mTiO_2$ (5 mg mL^{-1}) at 37 °C for 45 min with gentle shaking. Then, the mixture was separated by a magnetic field to remove the unbound bacteria. Negative staining was implemented for TEM measurement. In addition, the samples were fixed with 1 mL of 2.5% glutaraldehyde at 4 °C overnight, dehydrated with 25, 50, 75, and

DOI: 10.1021/acsami.6b06671
ACS Appl. Mater. Interfaces 2016, 8, 19371−19378

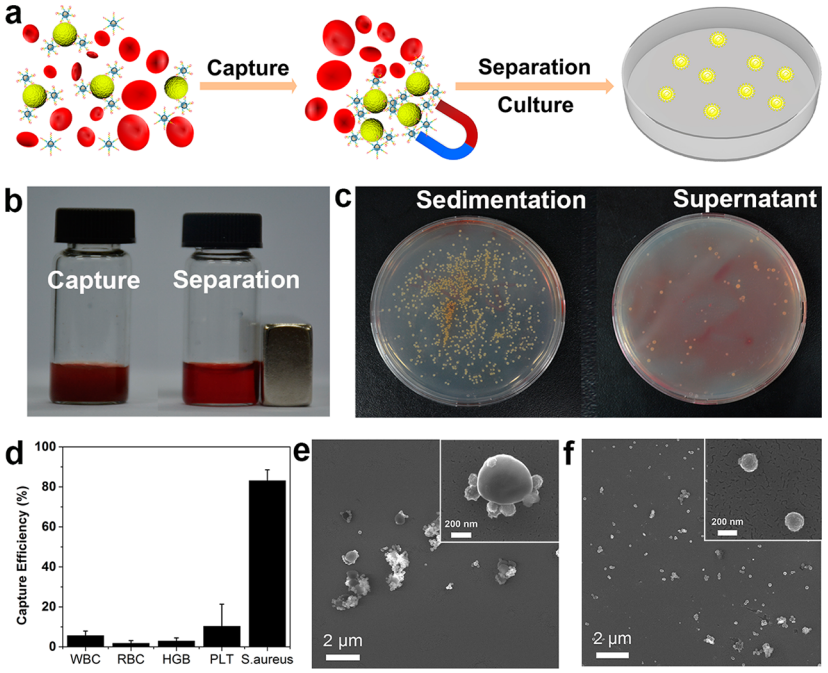

Figure 2. (a) Schematic illustration of the principle for pathogenic bacteria identification. (b) Photographs showing the capture of bacteria by Apt-Fe_3O_4@$mTiO_2$ nanoparticles (left) and the separation of bacteria from infected blood by a bar magnet (right). (c) Agar plates showing the amounts of *S. aureus* in sedimentation (left) and supernatant (right) after magnetic capture. (d) Capture efficiency of different compounds in blood after being treated with $Apt_{S.aureus}$-Fe_3O_4@$mTiO_2$. SEM images of *S. aureus* after incubated with (e) $Apt_{S.\ aureus}$-Fe_3O_4@ $mTiO_2$ and (f) $Apt_{E.\ coli}$-Fe_3O_4@ $mTiO_2$.

100% ethanol, and coated with a gold−palladium alloy to obtain the SEM photograph.

Selectivity Test of *S. aureus*. In a typical experiment, human blood was spiked with *S. aureus* to simulate BSI at a final concentration of 10^5 CFU mL^{-1}. Subsequently, 20 μL of aptamer-conjugated Fe_3O_4@$mTiO_2$ nanoparticles were added to the infected blood, and the mixture was incubated for 2 h with gentle shaking followed by magnetic separation. The numbers of *S. aureus* in the supernatant and sediment were determined by the colony counting method. Further, the concentrations of red blood cells, white blood cells, and platelets in the blood were monitored by routine blood tests.[54]

Cytotoxicity Test. The hydrophilic Fe_3O_4@$mTiO_2$ nanoparticles were incubated with *S. aureus* (10^5 CFU mL^{-1}) at 37 °C under gentle shaking. During incubation, bacterial viability was monitored by the colony counting method.[51]

Enrichment of Bacteria from Infected Blood Samples. The cultured *S. aureus* cells were spiked into healthy human blood with final concentrations of 10, 50, 10^2, 5×10^2, 10^3, and 2×10^3 CFU mL^{-1}. Then, 20 μL of aptamer-conjugated Fe_3O_4@$mTiO_2$ was added into the series of infected blood and incubated at 37 °C with continuous shaking. After 2 h of incubation, a bar magnet was used for the magnetic separation, and the enrichment efficiency was monitored by the colony counting method. The enrichment of *E. coli* in human blood was carried out under the same process by changing just the aptamer type.

Enrichment Kinetics Studies. A blood sample containing *S. aureus* (10^5 CFU mL^{-1}) was incubated with $Apt_{S.\ aureus}$-Fe_3O_4@$mTiO_2$. At different time intervals, the supernatant was collected to determine the concentration of *S. aureus* left in the supernatant. Bacterial enrichment efficiencies at different time periods were monitored by the colony counting method.

Bacterial Culture in Blood. In this experiment, 1 mL of human blood containing 50 CFU mL^{-1} *S. aureus* was added into 10 mL of LB broth and incubated at 37 °C under continuous shaking to observe the process of bacterial culture. At different time intervals during the incubation, 100 μL of the bacterial culture was taken out and spread out onto 3 agar plates. The bacterial growth condition was monitored by the colony counting method.[51]

RESULTS AND DISCUSSION

The Fe_3O_4@$mTiO_2$ nanoparticles were synthesized following the previously reported protocol.[45,46] XRD patterns were obtained to rigorously investigate the Fe_3O_4@$mTiO_2$ nanoparticles (Figure S2). Before calcination, the Fe_3O_4@$mTiO_2$ precursor (designated as Fe_3O_4@TiO_2) showed an XRD pattern similar to that of the typical structure of Fe_3O_4. No characteristic TiO_2 crystal peak was found, implying the formation of an amorphous TiO_2 shell. After calcination treatment, new XRD peaks were clearly observed and could be well-indexed to the formation of the anatase-phase TiO_2 shell. The energy dispersive X-ray (EDX) spectrum of the Apt-Fe_3O_4@$mTiO_2$ nanoparticles reveals the existence of Ti, Fe, and O, indicating that the obtained nanoparticles were composed of the target materials (Figure S3). To construct the aptamer-based capture platform, amino-labeled aptamer was introduced onto the surface of the prepared Fe_3O_4@ $mTiO_2$ nanoparticles through the glutaraldehyde spacer method (Figure 1a).[48,49] TEM images in Figure 1b showed that the obtained Apt-Fe_3O_4@$mTiO_2$ were well-dispersed in water with an average diameter of about 200 nm. The element distributions were also confirmed with X-ray mapping (Figure 1c), which suggested that a thin layer of TiO_2 was uniformly coated on the surface of the Fe_3O_4 nanoparticles. In the line scan analysis (Figure S5), the hemispherical shaped Kα1 spectral of O and Fe suggests that these two elements were almost uniformly distributed in the nanoparticles. The Ti Kα1 spectral profile indicates the encapsulation of the Fe_3O_4 core by the TiO_2 shell. The successful introduction of an aptamer onto the surface of the Fe_3O_4@$mTiO_2$ nanoparticles was verified by ζ-potential measurements (Figure S8).[55]

The interaction between the aptamer and bacteria was analyzed by confocal microscopy. Typically, FAM-labeled

DOI: 10.1021/acsami.6b06671
ACS Appl. Mater. Interfaces 2016, 8, 19371−19378

aptamers targeted to *S. aureus* (FAM-Apt$_{S.\ aureus}$) were incubated with *S. aureus* and *E. coli* suspensions, respectively. After removal of unbound FAM-Apt$_{S.\ aureus}$, the bacteria were resuspended in PBS buffer. Then the bacterial suspension was dropped on a glass slide and was visualized under confocal microscopy. The confocal imaging showed that the fluorescent dots and *S. aureus* in the bright field were well overlaid, indicating that FAM-Apt$_{S.\ aureus}$ exhibited favorable binding affinity to target *S. aureus* (Figure 1d). In sharp contrast, a fluorescence dot was not observed from *E. coli*, which was also treated with FAM-Apt$_{S.\ aureus}$ (Figure 1e). The results demonstrate that the aptamer binds to the target bacteria with strong affinity and does not cross-react with other bacterial species.[14] The binding ability of aptamer-conjugated Fe_3O_4@$mTiO_2$ nanoparticles was re-evaluated via TEM measurement.[37] The images in Figure 1f showed that several Fe_3O_4@$mTiO_2$ nanoparticles were tightly conjugated around the *S. aureus* cells, suggesting that the aptamer-conjugated Fe_3O_4@$mTiO_2$ nanoparticle has strong binding affinity for the target bacteria. The bacterial sensing ability of aptamer-conjugated Fe_3O_4@$mTiO_2$ was further investigated, and pure Fe_3O_4@$mTiO_2$ was used as a control. As shown in Figure 1g, over 89% of *S. aureus* in culture medium were captured by Apt$_{S.\ aureus}$-Fe_3O_4@$mTiO_2$. However, few bacteria were absorbed by pure Fe_3O_4@$mTiO_2$ nanoparticles. These results demonstrate the capability of aptamers to recognize and bind to target bacteria with high specificity and strong affinity.

As a real application, the ability of the aptamer-based capture platform to capture bacteria from human blood was investigated. Apt$_{S.\ aureus}$-Fe_3O_4@$mTiO_2$ nanoparticles were incubated with a blood sample spiked with *S. aureus* at a concentration of 10^5 CFU mL^{-1}. As shown in Figure 2a, *S. aureus* in blood can be captured by Apt$_{S.\ aureus}$-Fe_3O_4@$mTiO_2$ selectively and further separated under a magnetic field. The photograph in Figure 2b showed that bacteria-Fe_3O_4@$mTiO_2$ complexes could be easily separated from blood within 2 min by a bar magnet. Photographs of agar plates demonstrated that most of the *S. aureus* cells were captured by the aptamer-based capture platform, and few bacteria were present in the supernatant (Figure 2c). Colony counting results indicate that the capture efficiency of the capture platform for *S. aureus* was about 83% (Figure 2d). Further, the concentrations of WBC, RBC, HGB, and PLT in the blood showed little change after being treated with Apt$_{S.\ aureus}$-Fe_3O_4@$mTiO_2$ nanoparticles. The results imply that the designed aptamer-based capture platform features good capability to capture bacteria in whole human blood. The specific binding of the aptamer-based capture platform to bacterial cells in blood was verified by SEM.[40] SEM images in Figure 2e showed that *S. aureus* could be efficiently captured by the Apt$_{S.\ aureus}$-Fe_3O_4@$mTiO_2$ nanoparticles. In comparison, Fe_3O_4@$mTiO_2$ modified with the aptamer target to *E. coli* (designated as Apt$_{E.\ coli}$-Fe_3O_4@$mTiO_2$) showed much less binding to *S. aureus* (Figure 2f). Such good selectivity of the capture platform was ascribed to the fact that aptamers bind to targets through the formation of a sequence-defined unique structure.[31] Furthermore, the hydrophilic Fe_3O_4@$mTiO_2$ nanoparticles were incubated with an *S. aureus*-infected blood sample to investigate the cytotoxicity. Photographs of the cultured agar plates show extensive growth of *S. aureus*, and the bacterial viability remained at 100% during incubation (Figure S12), indicating that this capture platform has little effect on the activity of the target bacteria. Such good selectivity and activity-friendly characteristics of the capture platform make it appealing for capturing target bacteria from human blood samples.

As mentioned above, this aptamer-based capture platform could capture bacteria from blood samples with excellent capture efficiency at high concentrations; however, the infectious dose of bacteria in the real blood sample was very low (approximately 100 cells mL^{-1}).[12] To evaluate the capture sensitivity of the capture platform at low bacterial concentrations, human blood samples were spiked with *S. aureus* at different concentrations (10, 50, 100, 500, 1000, and 2000 CFU mL^{-1}). After that, appropriate amounts of Apt$_{S.\ aureus}$-Fe_3O_4@$mTiO_2$ were added to enrich the bacteria. The typical photographs of *S. aureus* colonies in Figure 3a show that the

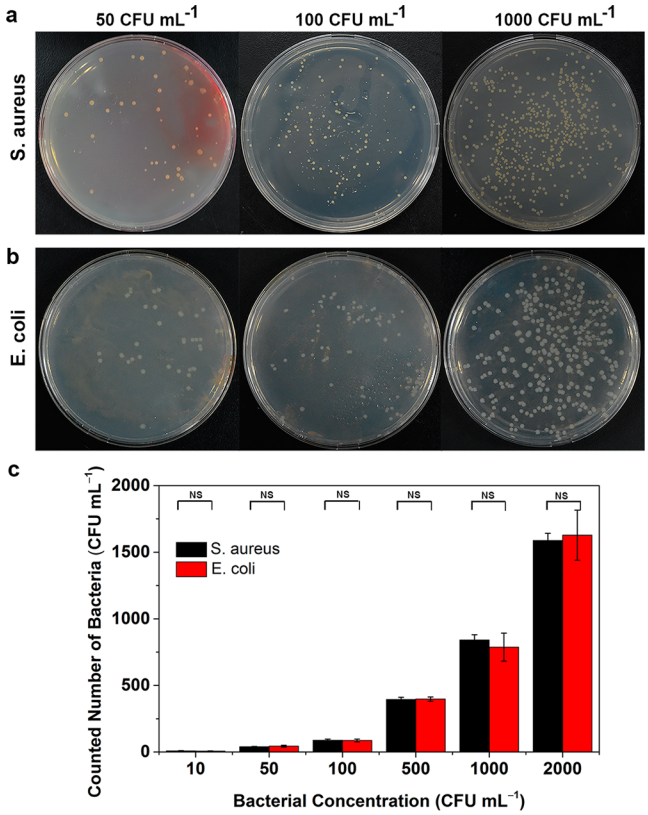

Figure 3. Photographs of agar plates onto which (a) *S. aureus* and (b) *E. coli* were cultivated after being enriched by the corresponding aptamer-based capture platform. (c) Actual counted cell numbers of *S. aureus* and *E. coli* versus a broad range of spiked bacteria concentrations. *p*-Values were calculated by the *t* test. $p > 0.05$ and * for $p < 0.05$, $n = 3$. NS = not significant.

number of *S. aureus* captured by Apt$_{S.\ aureus}$-Fe_3O_4@$mTiO_2$ increased as the concentration of added bacteria increased. The same results were also obtained for *E. coli* by changing just the aptamer type immobilized on Fe_3O_4@$mTiO_2$ nanoparticles (Figure 3b). It is noteworthy that both *S. aureus* and *E. coli* could be effectively enriched with high enrichment efficiency of about 80% even at a low detection range (Figures 3c, S13, and S14), thus indicating the generality of the feasibility of the capture platform for bacterial enrichment in clinical blood samples. The good performance of the capture platform was attributed to the high selectivity and strong affinity of the aptamers. These data suggest that the developed capture platform is sensitive enough to detect bacteria in the blood of a patient suffering from sepsis and bacteremia.

DOI: 10.1021/acsami.6b06671
ACS Appl. Mater. Interfaces 2016, 8, 19371−19378

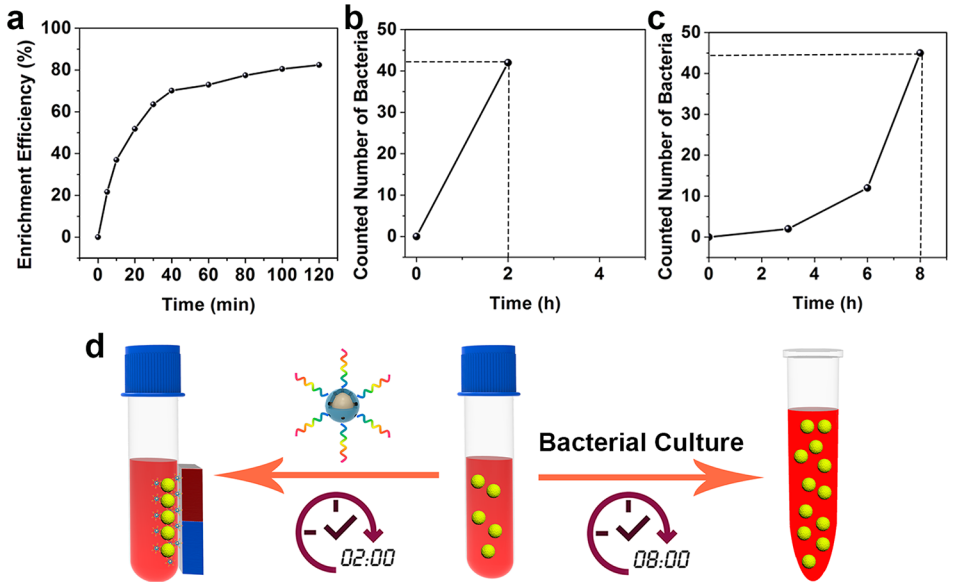

Figure 4. (a) Bacterial capture efficiency versus incubation time. A total of 10^4 CFU mL^{-1} bacteria were spiked into the blood. (b) The total time needed for the enrichment of *S. aureus* from human blood. (c) The time needed for bacterial growth to obtain the same colonies. (d) Schematic representation of the detection time for identifying pathogenic bacteria in human blood. Left: the aptamer-based capture platform. Right: bacterial culture.

Generally, during routine blood culture, the blood of the patient is added into a culture bottle and incubated within a continuous blood culture system. Bacterial growth is monitored by the production of metabolite in the culture bottle. It is time-consuming and usually requires several days to report the positive results. In our system, the patient blood samples are incubated with the aptamer-based capture platform for specific enrichment. Once exposed to the target bacteria, aptamers will bind to target bacteria with high selectivity and strong affinity. The complexes are further separated from the blood under a magnetic field, and the resulting bacteria will be inoculated on solid medium for colony counting and further tests. First, the bacterial enrichment kinetics with our capture platform were monitored by the colony counting method. The plots show that *S. aureus* spiked into blood could be enriched within 2 h with a final capture efficiency of 80% (Figure 4a). The result indicates that 2 h is enough to guarantee high capture efficiency. The time to detection (TTD) of the bloodstream infection was further investigated both in traditional bacterial culture and the developed capture platform. Bacterial capture and growth were both monitored by plate counting methods. In detail, an *S. aureus*-infected blood sample was treated with $Apt_{S.aureus}$-Fe_3O_4@mTiO_2 for bacteria-specific enrichment. Meanwhile, an equal volume of infected blood was added into an LB medium to observe bacterial growth. After 2 h of incubation, nearly all of the bacteria added into the blood were enriched by the capture platform. In contrast, it took more than 8 h for bacterial growth to obtain the same colonies (Figures 4b and c). The TTD of the bacterial bloodstream infection for the developed capture platform could be effectively shortened in comparison to the gold standard method in clinical diagnosis of BSI (Figure 4d), which needs several days to report positive bacterial growth. Accordingly, our designed capture platform features rapid bacterial detection capability and may be a substitute for the first step in blood culture to shorten the time needed to reach a definitive bacterial identification.

CONCLUSIONS

In summary, we demonstrated the feasibility of the designed aptamer-based capture platform for rapid and selective detection of BSI as well as pathogen identification in bacteremia and sepsis. The results show that the capture platform is capable of capturing and enriching bacteria from human blood with high selectivity and strong binding affinity and has a negligible effect on the activity of captured bacteria. In addition, the capture platform features adaptable bacterial enrichment efficiency of about 80% even at low bacterial concentrations ranging from 10 to 2000 CFU mL^{-1}, thus indicating the feasibility of enrichment and detection of bacteria in clinical samples. More importantly, the bacteria can be enriched and separated within 2 h, and the time for bacterial identification is effectively shortened in comparison to the gold standard method in the clinical diagnosis of BSI. Therefore, the capture platform allows rapid and sensitive detection of pathogenic bacteria and may contribute to administering effective antibiotic therapy at an early stage. It is worth noting that this capture platform is able to concentrate different targets from human blood by changing only the aptamer types, indicating that the detection of any pathogenic bacteria will be possible with this approach. It is envisioned that this strategy may pave a way for the detection of biomarkers and find potential applications in disease diagnosis.

ASSOCIATED CONTENT

Supporting Information

The Supporting Information is available free of charge on the ACS Publications website at DOI: 10.1021/acsami.6b06671.

TEM characterization, SEM characterization, XRD patterns, EDX spectrum, ζ-potentials, bacterial colony counting results, and details on chemicals and instruments (PDF)

DOI: 10.1021/acsami.6b06671
ACS Appl. Mater. Interfaces 2016, 8, 19371−19378

AUTHOR INFORMATION

Corresponding Author

* E-mail: yuanquan@whu.edu.cn.

Notes

The authors declare no competing financial interest.

ACKNOWLEDGMENTS

This work was supported by the National Natural Science Foundation of China (Grants 51272186 and 21422105), "A Foundation for the Author of National Excellent Doctoral Dissertation of P. R. China" (Grant 201220), and Ten Thousand Talents Program for Young Talents. Q.Y. thanks the large-scale instrument and equipment sharing foundation of Wuhan University.

REFERENCES

(1) Cohen, J. The Immunopathogenesis of Sepsis. *Nature* **2002**, *420*, 885−891.

(2) Angus, D. C.; van der Poll, T. Severe Sepsis and Septic Shock. *N. Engl. J. Med.* **2013**, *369*, 840−851.

(3) Rocheteau, P.; Chatre, L.; Briand, D.; Mebarki, M.; Jouvion, G.; Bardon, J.; Crochemore, C.; Serrani, P.; Lecci, P. P.; Latil, M.; Matot, B.; Carlier, P. G.; Latronico, N.; Huchet, C.; Lafoux, A.; Sharshar, T.; Ricchetti, M.; Chretien, F. Sepsis Induces Long-Term Metabolic and Mitochondrial Muscle Stem Cell Dysfunction Amenable by Mesenchymal Stem Cell Therapy. *Nat. Commun.* **2015**, *6*, 10145.

(4) Hidron, A. I.; Edwards, J. R.; Patel, J.; Horan, T. C.; Sievert, D. M.; Pollock, D. A.; Fridkin, S. K. Antimicrobial-Resistant Pathogens Associated with Healthcare-Associated Infections: Annual Summary of Data Reported to the National Healthcare Safety Network at the Centers for Disease Control and Prevention, 2006−2007. *Infect. Cont. Hosp. Ep.* **2008**, *29*, 996−1011.

(5) Zhu, L. X.; Shen, D. X.; Zhou, Q. M.; Liu, C. J.; Li, Z. X.; Fang, X. D.; Li, Q. Z. Universal Probe Library Based Real-time PCR for Rapid Detection of Bacterial Pathogens from Positive Blood Culture Bottles. *World J. Microbiol. Biotechnol.* **2014**, *30*, 967−975.

(6) Ray, P. C.; Khan, S. A.; Singh, A. K.; Senapati, D.; Fan, Z. Nanomaterials for Targeted Detection and Photothermal Killing of Bacteria. *Chem. Soc. Rev.* **2012**, *41*, 3193−3209.

(7) Lee, A.; Mirrett, S.; Reller, L. B.; Weinstein, M. P. Detection of Bloodstream Infections in Adults: How Many Blood Cultures Are Needed? *J. Clin. Microbiol.* **2007**, *45*, 3546−3548.

(8) Reisner, B. S.; Woods, G. L. Times to Detection of Bacteria and Yeasts in BACTEC 9240 Blood Culture Bottles. *J. Clin. Microbiol.* **1999**, *37*, 2024−2026.

(9) Sarkar, S.; Bhagat, I.; DeCristofaro, J. D.; Wiswell, T. E.; Spitzer, A. R. A Study of the Role of Multiple Site Blood Cultures in the Evaluation of Neonatal Sepsis. *J. Perinatol.* **2006**, *26*, 18−22.

(10) Saito, T.; Aoki, Y.; Mori, Y.; Kohi, F. Blood Culture Examinations at a Community Hospital Without a Microbiology Laboratory: Using an Automated Blood Culture System and Performing a Gram Stain on Positive Culture Bottles in the Institution. *J. Infect. Chemother.* **2004**, *10*, 239−241.

(11) Khan, S. A.; Singh, A. K.; Senapati, D.; Fan, Z.; Ray, P. C. Bioconjugated Popcorn Shaped Gold Nanoparticles for Targeted Photothermal Killing of Multiple Drug Resistant Salmonella DT104. *J. Mater. Chem.* **2011**, *21*, 17705−17709.

(12) Fan, Z.; Senapati, D.; Khan, S. A.; Singh, A. K.; Hamme, A.; Yust, B.; Sardar, D.; Ray, P. C. Popcorn-Shaped Magnetic Core-Plasmonic Shell Multifunctional Nanoparticles for the Targeted Magnetic Separation and Enrichment, Label-Free SERS Imaging, and Photothermal Destruction of Multidrug-Resistant Bacteria. *Chem. - Eur. J.* **2013**, *19*, 2839−2847.

(13) Kavruk, M.; Celikbicak, O.; Ozalp, V. C.; Borsa, B. A.; Hernandez, F. J.; Bayramoglu, G.; Salih, B.; Arica, M. Y. Antibiotic Loaded Nanocapsules Functionalized with Aptamer Gates for Targeted Destruction of Pathogens. *Chem. Commun.* **2015**, *51*, 8492−8495.

(14) Boedicker, J. Q.; Li, L.; Kline, T. R.; Ismagilov, R. F. Detecting Bacteria and Determining Their Susceptibility to Antibiotics by Stochastic Confinement in Nanoliter Droplets Using Plug-based Microfluidics. *Lab Chip* **2008**, *8*, 1265−1272.

(15) Yealy, D. M.; Kellum, J. A.; Huang, D. T.; Barnato, A. E.; Weissfeld, L. A.; Pike, F.; Terndrup, T.; Wang, H. E.; Hou, P. C.; LoVecchio, F.; Filbin, M. R.; Shapiro, N. I.; Angus, D. C. A Randomized Trial of Protocol-Based Care for Early Septic Shock. *N. Engl. J. Med.* **2014**, *370*, 1683−1693.

(16) Niemz, A.; Ferguson, T. M.; Boyle, D. S. Point-of-care Nucleic Acid Testing for Infectious Diseases. *Trends Biotechnol.* **2011**, *29*, 240−250.

(17) Shepard, J. R.; Addison, R. M.; Alexander, B. D.; Della-Latta, P.; Gherna, M.; Haase, G.; Hall, G.; Johnson, J. K.; Merz, W. G.; Peltroche-Llacsahuanga, H.; Stender, H.; Venezia, R. A.; Wilson, D.; Procop, G. W.; Wu, F.; Fiandaca, M. J. Multicenter Evaluation of the *Candida albicans*/*Candida glabrata* Peptide Nucleic Acid Fluorescent *in situ* Hybridization Method for Simultaneous Dual-Color Identification of *C. albicans* and *C. glabrata* Directly from Blood Culture Bottles. *J. Clin. Microbiol.* **2008**, *46*, 50−55.

(18) Wang, P. Rapid Differentiation of *Candida albicans* from non-*C. albicans* Directly in a Variety of Clinical Specimens Using Fluorescent *in situ* Hybridisation. *Mycoses* **2011**, *54*, 331−336.

(19) Burtscher, C.; Wuertz, S. Evaluation of the Use of PCR and Reverse Transcriptase PCR for Detection of Pathogenic Bacteria in Biosolids from Anaerobic Digestors and Aerobic Composters. *Appl. Environ. Microb.* **2003**, *69*, 4618−4627.

(20) Ottesen, E. A.; Hong, J. W.; Quake, S. R.; Leadbetter, J. R. Microfluidic Digital PCR Enables Multigene Analysis of Individual Environmental Bacteria. *Science* **2006**, *314*, 1464−1467.

(21) Pechorsky, A.; Nitzan, Y.; Lazarovitch, T. Identification of Pathogenic Bacteria in Blood Cultures: Comparison Between Conventional and PCR Methods. *J. Microbiol. Methods* **2009**, *78*, 325−330.

(22) Zhang, L.; Xu, J. J.; Mi, L.; Gong, H.; Jiang, S. Y.; Yu, Q. M. Multifunctional Magnetic-Plasmonic Nanoparticles for Fast Concentration and Sensitive Detection of Bacteria Using SERS. *Biosens. Bioelectron.* **2012**, *31*, 130−136.

(23) Shi, M. L.; Zheng, J.; Tan, Y. J.; Tan, G. X.; Li, J. S.; Li, Y. H.; Li, X.; Zhou, Z. G.; Yang, R. H. Ultrasensitive Detection of Single Nucleotide Polymorphism in Human Mitochondrial DNA Utilizing Ion-Mediated Cascade Surface-Enhanced Raman Spectroscopy Amplification. *Anal. Chem.* **2015**, *87*, 2734−2740.

(24) Wang, H. Y.; Zhou, Y. F.; Jiang, X. X.; Sun, B.; Zhu, Y.; Wang, H.; Su, Y. Y.; He, Y. Simultaneous Capture, Detection, and Inactivation of Bacteria as Enabled by a Surface-Enhanced Raman Scattering Multifunctional Chip. *Angew. Chem., Int. Ed.* **2015**, *54*, 5132−5136.

(25) Chung, H. J.; Reiner, T.; Budin, G.; Min, C.; Liong, M.; Issadore, D.; Lee, H.; Weissleder, R. Ubiquitous Detection of Gram-Positive Bacteria with Bioorthogonal Magnetofluorescent Nanoparticles. *ACS Nano* **2011**, *5*, 8834−8841.

(26) Miranda, O. R.; Li, X. N.; Garcia-Gonzalez, L.; Zhu, Z. J.; Yan, B.; Bunz, U. H.; Rotello, V. M. Colorimetric Bacteria Sensing Using a Supramolecular Enzyme-Nanoparticle Biosensor. *J. Am. Chem. Soc.* **2011**, *133*, 9650−9653.

(27) Shangguan, J. F.; Li, Y. H.; He, D. G.; He, X. X.; Wang, K. M.; Zou, Z.; Shi, H. A Combination of Positive Dielectrophoresis Driven On-line Enrichment and Aptamer-Fluorescent Silica Nanoparticle Label for Rapid and Sensitive Detection of *Staphylococcus aureus*. *Analyst* **2015**, *140*, 4489−4497.

(28) Kang, D. K.; Ali, M. M.; Zhang, K. X.; Huang, S. S.; Peterson, E.; Digman, M. A.; Gratton, E.; Zhao, W. Rapid Detection of Single Bacteria in Unprocessed Blood Using Integrated Comprehensive Droplet Digital Detection. *Nat. Commun.* **2014**, *5*, 5427.

DOI: 10.1021/acsami.6b06671
ACS Appl. Mater. Interfaces 2016, 8, 19371−19378

(29) Lee, H.; Yoon, T. J.; Weissleder, R. Ultrasensitive Detection of Bacteria Using Core-Shell Nanoparticles and an NMR-Filter System. *Angew. Chem., Int. Ed.* **2009**, *48*, 5657−5660.
(30) Liu, J. W.; Cao, Z. H.; Lu, Y. Functional Nucleic Acid Sensors. *Chem. Rev.* **2009**, *109*, 1948−1998.
(31) Wang, J.; Shen, H. J.; Hu, X. X.; Li, Y.; Li, Z. H.; Xu, J. F.; Song, X. F.; Zeng, H. B.; Yuan, Q. A Targeted "Capture" and "Removal" Scavenger toward Multiple Pollutants for Water Remediation based on Molecular Recognition. *Adv. Sci.* **2016**, *3*, 1500289.
(32) Zheng, J.; Bai, J. H.; Zhou, Q. F.; Li, J. S.; Li, Y. H.; Yang, J. F.; Yang, R. H. DNA-Templated *in situ* Growth of AgNPs on SWNTs: A New Approach for Highly Sensitive SERS Assay of microRNA. *Chem. Commun.* **2015**, *51*, 6552−6555.
(33) Zhu, G. Z.; Zheng, J.; Song, E. Q.; Donovan, M.; Zhang, K. J.; Liu, C.; Tan, W. H. Self-assembled, Aptamer-tethered DNA Nanotrains for Targeted Transport of Molecular Drugs in Cancer Theranostics. *Proc. Natl. Acad. Sci. U. S. A.* **2013**, *110*, 7998−8003.
(34) Guo, W.; Hong, F.; Liu, N. N.; Huang, J. Y.; Wang, B. Y.; Duan, R. X.; Lou, X. D.; Xia, F. Target-Specific 3D DNA Gatekeepers for Biomimetic Nanopores. *Adv. Mater.* **2015**, *27*, 2090−2095.
(35) Lin, L. S.; Cong, Z.-X.; Cao, J.-B.; Ke, K. M.; Peng, Q.-L.; Gao, J. H.; Yang, H. H.; Liu, G.; Chen, X. Y. Multifunctional Fe_3O_4@ Polydopamine Core Shell Nanocomposites for Intracellular mRNA Detection and Imaging-Guided Photothermal Therapy. *ACS Nano* **2014**, *8*, 3876−3883.
(36) Chen, F.; Zhou, J.; Luo, F. L.; Mohammed, A. B.; Zhang, X.-L. Aptamer from Whole-Bacterium SELEX as New Therapeutic Reagent Against Virulent *Mycobacterium tuberculosis*. *Biochem. Biophys. Res. Commun.* **2007**, *357*, 743−748.
(37) Zhang, C. X.; Lv, X. F.; Han, X.; Man, Y.; Saeed, Y.; Qing, H.; Deng, Y. L. Whole-Cell based Aptamer Selection for Selective Capture of Microorganisms using Microfluidic Devices. *Anal. Methods* **2015**, *7*, 6339−6345.
(38) Wu, S. J.; Duan, N.; Shi, Z.; Fang, C. C.; Wang, Z. P. Simultaneous Aptasensor for Multiplex Pathogenic Bacteria Detection Based on Multicolor Upconversion Nanoparticles Labels. *Anal. Chem.* **2014**, *86*, 3100−3107.
(39) Wang, J. F.; Wu, X. Z.; Wang, C. W.; Shao, N. S.; Dong, P. T.; Xiao, R.; Wang, S. Q. Magnetically Assisted Surface-Enhanced Raman Spectroscopy for the Detection of *Staphylococcus aureus* Based on Aptamer Recognition. *ACS Appl. Mater. Interfaces* **2015**, *7*, 20919−20929.
(40) Cheng, D.; Yu, M. Q.; Fu, F.; Han, W. Y.; Li, G.; Xie, J. P.; Song, Y.; Swihart, M. T.; Song, E. Q. Dual Recognition Strategy for Specific and Sensitive Detection of Bacteria Using Aptamer-Coated Magnetic Beads and Antibiotic-Capped Gold Nanoclusters. *Anal. Chem.* **2016**, *88*, 820−825.
(41) Luo, C. H.; Lei, Y. N.; Yan, L.; Yu, T. X.; Li, Q.; Zhang, D. C.; Ding, S. J.; Ju, H. X. A Rapid and Sensitive Aptamer-Based Electrochemical Biosensor for Direct Detection of *Escherichia ColiO111*. *Electroanalysis* **2012**, *24*, 1186−1191.
(42) Chang, Y. C.; Yang, C. Y.; Sun, R. L.; Cheng, Y. F.; Kao, W. C.; Yang, P. C. Rapid Single Cell Detection of *Staphylococcus aureus* by Aptamer-Conjugated Gold Nanoparticles. *Sci. Rep.* **2013**, *3*, 1863.
(43) Li, W.; Yang, J. P.; Wu, Z. X.; Wang, J. X.; Li, B.; Feng, S. S.; Deng, Y. H.; Zhang, F.; Zhao, D. Y. A Versatile Kinetics-Controlled Coating Method to Construct Uniform Porous TiO_2 Shells for Multifunctional Core-Shell Structures. *J. Am. Chem. Soc.* **2012**, *134*, 11864−11867.
(44) Liu, J.; Sun, Z. K.; Deng, Y. H.; Zou, Y.; Li, C. Y.; Guo, X. H.; Xiong, L. Q.; Gao, Y.; Li, F. Y.; Zhao, D. Y. Highly Water-Dispersible Biocompatible Magnetite Particles with Low Cytotoxicity Stabilized by Citrate Groups. *Angew. Chem., Int. Ed.* **2009**, *48*, 5875−5879.
(45) Yue, Q.; Li, J. L.; Luo, W.; Zhang, Y.; Elzatahry, A. A.; Wang, X. Q.; Wang, C.; Li, W.; Cheng, X. W.; Alghamdi, A.; Abdullah, A. M.; Deng, Y. H.; Zhao, D. Y. An Interface Coassembly in Biliquid Phase: Toward Core-Shell Magnetic Mesoporous Silica Microspheres with Tunable Pore Size. *J. Am. Chem. Soc.* **2015**, *137*, 13282−13289.
(46) Li, W.; Deng, Y. H.; Wu, Z. X.; Qian, X. F.; Yang, J. P.; Wang, Y.; Gu, D.; Zhang, F.; Tu, B.; Zhao, D. Y. Hydrothermal Etching Assisted Crystallization: A Facile Route to Functional Yolk-Shell Titanate Microspheres with Ultrathin Nanosheets-Assembled Double Shells. *J. Am. Chem. Soc.* **2011**, *133*, 15830−15833.
(47) Deng, Y. H.; Cai, Y.; Sun, Z. K.; Zhao, D. Y. Magnetically Responsive Ordered Mesoporous Materials: A Burgeoning Family of Functional Composite Nanomaterials. *Chem. Phys. Lett.* **2011**, *510*, 1−13.
(48) Neely, A.; Perry, C.; Varisli, B.; Singh, A. K.; Arbneshi, T.; Senapati, D.; Kalluri, J. R.; Ray, P. C. Ultrasensitive and Highly Selective Detection of Alzheimer's Disease Biomarker Using Two-Photon Rayleigh Scattering Properties of Gold Nanoparticle. *ACS Nano* **2009**, *3*, 2834−2840.
(49) Singh, A. K.; Senapati, D.; Wang, S. G.; Griffin, J.; Neely, A.; Candice, P.; Naylor, K. M.; Varisli, B.; Kalluri, J. R.; Ray, P. C. Gold Nanorod Based Selective Identification of *Escherichia coli* Bacteria Using Two-Photon Rayleigh Scattering Spectroscopy. *ACS Nano* **2009**, *3*, 1906−1912.
(50) Li, W.; Yue, Q.; Deng, Y. H.; Zhao, D. Y. Ordered Mesoporous Materials Based on Interfacial Assembly and Engineering. *Adv. Mater.* **2013**, *25*, 5129−5152.
(51) Reasoner, D. J. Heterotrophic Plate Count Methodology in the United States. *Int. J. Food Microbiol.* **2004**, *92*, 307−315.
(52) Peñuelas-Urquides, K.; Villarreal-Treviño, L.; Silva-Ramírez, B.; Rivadeneyra-Espinoza, L.; Said-Fernández, S.; León, M. Measuring of *Mycobacterium tuberculosis* Growth. A Correlation of the Optical Measurements with Colony Forming Units. *Braz. J. Microbiol.* **2013**, *44*, 287−290.
(53) Zhang, Z. H.; Liu, C. H.; Bai, J. H.; Wu, C. C.; Xiao, Y.; Li, Y. H.; Zheng, J.; Yang, R. H.; Tan, W. H. Silver Nanoparticle Gated, Mesoporous Silica Coated Gold Nanorods (AuNR@MS@AgNPs): Low Premature Release and Multifunctional Cancer Theranostic Platform. *ACS Appl. Mater. Interfaces* **2015**, *7*, 6211−6219.
(54) Hans Gulliksson, H.; van der Meer, P. F. Storage of Whole Blood Overnight in Different Blood Bags Preceding Preparation of Blood Components: *in vitro* Effects on Red Blood Cells. *Blood Transfus* **2009**, *7*, 210−215.
(55) Song, H.; Nor, Y. A.; Yu, M. H.; Yang, Y. N.; Zhang, J.; Zhang, H. W.; Xu, C.; Mitter, N.; Yu, C. Z. Silica Nanopollens Enhance Adhesion for Long-Term Bacterial Inhibition. *J. Am. Chem. Soc.* **2016**, *138*, 6455−6462.

DOI: 10.1021/acsami.6b06671
ACS Appl. Mater. Interfaces 2016, 8, 19371−19378